Juhani Kristian Julin

Reducing 1/f noise in Al–AlO_x–Al tunnel junctions by thermal annealing

Master's Thesis

October 1, 2009

University of Jyväskylä

Nanoscience Center

Department of Physics

Contents

Acknowledgments

I would like to thank my executive supervisor Prof. Ilari Maasilta for opportunity to work here and my instructor Dr. Panu Koppinen for his advices and instructions to accomplish this project. It has been a privilege to work with so authoritative researcher, his guidance has been rewarding. My compliments to the research team and fellow personnel in Nanoscience Center I have met.

Author's contribution

The author of this thesis has done the sample fabrication, measurements and data analysis. The time spent was educative since this project was author's first contribution to nano sciences e.g. the cleanroom processes and the sensitive treatment of tunnel junctions that broke down easily. Several thousands of junctions were fabricated, but sample fabrication was, however, the easiest part, since low frequency noise measurements took long time, as the author built the measurement setup from scratch with testing different combinations. Essential milestones are described in this thesis.

Chapter 1

Introduction

Noise is usually considered as something to avoid. The meaning of "noise" may be interpreted as a neighbor's poor taste of music or the sound of motorway. Noise is also present in all electronics, especially when processing weak signals. It hinders remote broadcasting and communications.

Everybody is familiar with a crackle coming from a car radio when traveled far away from the nearest tower. It is not because of absolute noise level is increased, but the signal level is decreased in respect to the background noise. Nowadays radio is almost the only analog device since TV and telecommunications like mobile phones are digitized. Digital transmission, especially with some sort of error correction applied, is much more tolerant against the noise, but eventually too high noise level will block the signal.

In a laboratory, noise is also present, which is usually an unwanted scenario. One might want to measure, for example, a neutrino flux through the Earth, but since neutrinos interact weakly with matter, sensors show mostly noise. If a neurologist wants to study patient's brain functions, he or she might want to use SQUIDs, which are sensitive to very weak magnetic fields [1]. A noisy measurement setup might wreck any measurement, and the quality of the setup is as good as the weakest component of the setup.

Regardless of all the disadvantages of noise, it is essential to study just the noise. By understanding the noise, one may gain vital information of the structure of the material, e.g. properties of charge transport channels. There exist several different noise sources, which are briefly discussed in the following chap-

ter.

The main subject here was to study the low frequency noise called 1/f-noise. The one motivation to study 1/f noise in Al–AlO_x–Al tunnel junctions is the possible use of tunnel junctions in quantum computation. Superconducting tunnel junctions (Josephson junctions) may be used as a solid state realization of a qubit [2]. Decoherence due to external sources eventually causes superposition to collapse with some dephasing time. Different methods for decoherence exists: for example the Josephson energy fluctuates in time because of imperfections in barrier, which also influences on qubit potential energy [3]. The 1/f noise may emerge from the substrate or tunneling barrier, thus by decreasing the 1/f noise the qubit decoherence will be decreased.

One method already known to stabilize tunnel junctions is thermal annealing [4]. Now, the impact on noise was studied by measuring the 1/f noise before and after annealing. Because qubits operate at millikelvin temperature the noise was also measured at different temperatures to study temperature dependence, but no sub-kelvin measurements were done in this thesis.

Noise measurements were also done for junctions fabricated on different substrates, silicon oxide and silicon nitride (SiO and SiN) to check whether the noise depends on it.

Most of the samples were fabricated in an ultra high vacuum (UHV) conditions to minimize contamination of junctions. Some samples were intentionally fabricated in high vacuum (HV) capable evaporator to check whether the noise depends on metal deposition cleanliness.

Chapter 2

Theory

2.1 Theoretical background of noise mechanisms

Noise is not only a random background to disturb life in laboratory, but a physical signature of the sample. It depends on the material, temperature and other prevailing conditions [5]. Noise can be measured by detecting e.g. voltage fluctuations but the physical background from which they are emerging may vary.

Some sources of noise are theoretically well understood, some other are not. Here is a brief introduction to different noise mechanisms with quantitative formulas explained, if any available.

2.1.1 Johnson noise

Let us at first consider Johnson noise, which is uniform at all frequencies. Such a noise, whose amplitude is the same at all frequencies, is called white noise, i.e. it is frequency independent noise.

Johnson noise is due to thermal fluctuations of electrons, which produce a "viscous frictions", or energy loss seen as a random voltage output. It is interesting to note that any physical analog of the resistance has fluctuations due to the fluctuation-dissipation phenomenon, so that the Johnson noise is just a special case [6].

Johnson noise is always present, with or without a voltage bias. It is the ultimate minimal noise level in any component, a physical fact that cannot be avoided. Other noise sources may possibly be reduced all the way down to John-

son level [6].

J. B. Johnson and H. Nyquist first investigated this noise experimentally in 1928 [7]. Nyquist's theorem states that the power spectral density of voltage fluctuation across a resistor R at temperature T is [5]

$$S_V(f) = 4k_BTR, \tag{2.1}$$

where k_B is the Boltzmann's constant. S_V is in units of V^2/Hz.

2.1.2 Shot noise

Shot noise arises from the discrete charge of the electron, which can be demonstrated for example by sensitively measuring current spectrum while electrons travel from the cathode to the anode. The equation is for the spectral density of shot noise (Schottky, 1918) [8]

$$S_I(f) = 2eI, \tag{2.2}$$

where e is the charge of the electron and I is the constant current across the device. Notice here that the noise is expressed as current noise S_I, unlike for the Johnson noise, where it was purely voltage noise due to its independence on bias.

2.1.3 1/f noise

In 1925, Johnson found frequency dependent noise whose spectral density increased with decreasing frequency [9]. Schottky postulated that it emerges from some slow random motion and named it a "flicker noise". Similar type of current noise has been found from many different electrical components and its spectrum is inversely proportional to the frequency f. This type of noise has equal power per decade of frequency and is often referred to as a pink noise, but most commonly just 1/f noise. Even down to very low frequencies, this noise obeys the rule it was named after.

Low frequency measurements are naturally time consuming: measuring one data point at 1 Hz takes time at least one second and for a spectrum there must be several points. For a reliable data gathering, averaging must be used to eliminate

unwanted peaks and distortion. Despite these technical difficulties, 1/f noise was measured down to below a micro-hertz [10].

The source of 1/f noise has been mystery all the time, it is still without commonly accepted theory although many experimental results have come out. One characteristic feature is that 1/f noise is mostly present in conductors with small dimensions, e.g. a thick wire resistor does not possess high 1/f noise while a thin nanowire does. Evidences indicate that the 1/f noise might emerge from electron trapping into and out of vacancies in lattice, which might take place in a substrate or inside a tunneling barrier. As seen later, 1/f noise in carbon resistors is negligible compared to noise in tunnel junctions, which contains a well defined dielectric barrier [11].

2.1.4 Dependence on current

1/f noise is, like shot noise, a modulation noise whose voltage power spectral density is proportional to the square of the voltage V applied over the sample. It obeys Ohm's law $S_V \propto V^2 \propto I^2$.

To study the characteristic noise in sample independent of the value of current flow through the sample, resistance noise can be introduced. It is defined, based on the assumption of Ohmic behavior of the resistor, as voltage noise divided by bias current over the sample. It leads to the formula [5]

$$\frac{S_R(f)}{R_S^2} = \frac{S_V(f)}{V_S^2}, \tag{2.3}$$

where S_R is the resistance noise power spectral density, R_S the sample resistance, S_V the voltage noise power spectral density and V_S the voltage over the sample. S_R has units Ω^2/Hz.

2.1.5 Hooge formula

It has been found that 1/f noise often follows $f^{-\gamma}$ power law with the exponent $\gamma \approx 1$. In addition, the Ohm's law holds well. Using this knowledge, Hooge analyzed data from different devices obtained by different authors and discovered the correlation between them. He introduced his famous empirical relationship

[9]

$$\frac{S_V(f)}{V_S^2} = \frac{\alpha}{N_c f}, \tag{2.4}$$

where N_c is the total number of free charge carriers in the sample and α is an empirical constant. Via data analysis he acquired α to be approximately $2 \cdot 10^{-3}$ [12].

The term N_c in Hooge's formula explains the noise increase while reducing the size of the sample. When reducing the size, available conducting channels decreases which affects the N_c term of free charge carriers.

Later on, it was found for some materials that the constant α varies orders of magnitude from the original value, and that the exponent γ is not necessarily exactly one. Hooge's relation is however functional in many cases, so it has not been dismissed yet.

2.2 Tunnel junctions

Tunneling is one of the very basic phenomena in quantum mechanics. It states a particle, which is also a delocalized wave function, can penetrate through classically forbidden regions. This is realized for electrons in tunnel junctions [13].

In a tunnel junction, there exists a narrow layer of dielectric material between conducting electrodes. The barrier prevents classical electrical conducting through the junction at low temperatures, but with certain probabilities the electrons can tunnel through the insulating barrier and a net current is achieved. The barrier thickness is commonly couple of nanometers (1–2 nm) [14].

2.2.1 NIN tunneling

Here normal-metal to normal-metal (NIN) tunneling is explained briefly. Tunneling is commonly approximated by a trapezoidal potential barrier (see Fig. 2.1), where an elastic tunneling can happen only horizontally [15]. Electron can tunnel to the opposite site only if there is a free energy state at the same energy than tunneling electron has. Tunneling current is [13]

$$I \propto |\tau|^2 \int_{-\infty}^{\infty} N_1(E) N_2(E + eV)[f(E) - f(E + eV)]dE, \tag{2.5}$$

where V is voltage across the junction, $N_1(E)$ and $N_2(E + eV)$ are densities of states at different sides of the junction, f is the Fermi-Dirac distribution and $|\tau|^2$ is tunneling probability.

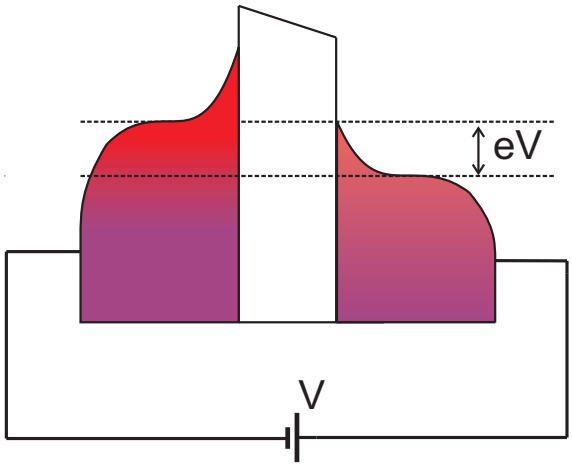

Figure 2.1: Tunneling barrier in a tunnel junction is approximated by a trapezoidal barrier. On each side, the temperature dependent electron state configuration is illustrated. Net current is achieved when bias voltage is applied over the junction.

With zero bias voltage, the net current is zero. Electrons can tunnel through the barrier but no net flow is achieved. When a voltage is applied over the junction, Fermi distributions are altered so that the energy levels are shifted with respect to each other. Now tunneling is not the same for both directions, and there is a net current through the junction. At zero temperature and at low bias the current has a form [13]

$$I_{nn} = \frac{2eA}{h}|\tau|^2 N_1(0)N_2(0)eV \equiv G_{nn}V, \tag{2.6}$$

where A is cross-section area in junction, h is Planck constant, $N_1(0)$ and $N_2(0)$ are densities of states of free electrons on the Fermi surfaces and G_{nn} is the tunneling conductance of the junction.

In the above formula, one can see that the current depends on a few parameters. Tunneling matrix element is a material specific quantum mechanical entity containing the barrier properties e.g. dependence on thickness and height of the barrier. Current is of course proportional to junction area because there is more cross sectional space for tunneling to take place. Voltage dependence is also trivial since it shifts the chemical potential of electrons. Temperature dependence is

concealed inside the Fermi functions. It is vital to notice that the conductance of tunnel junction increases while increasing temperature and this temperature dependence is a good sign of the presence of a real tunnel junction. For example, a typical resistance decrease for a cool-down from 300 K to 77 K is about 15 % [16]. Recall that for most common metals the conductance increases while decreasing the temperature, and eventually some materials become superconducting.

At higher bias, tunneling conductance depends also on the bias voltage. In an idealized case, i.e. by assuming a trapezoidal barrier and that direct tunneling dominates, the tunneling conductance may be expressed using the WKB approximation [15]

$$G = G_0[1 + (V/V_0)^2], \tag{2.7}$$

where $V_0^2 = 4\hbar^2/(e^2 m)\phi_0/x_0$, $G_0 = e^2 A\sqrt{2m\phi_0}/(h^2 x_0)\exp(-2x_0\sqrt{2m\phi_0}/\hbar)$, A is junction area, ϕ_0 is the barrier height and x_0 barrier thickness.

Tunnel junctions are versatile devices for many applications. They have many interesting properties to study fundamental physical phenomena, especially when fabricated out of different materials. One very common application is a NIS junction with a superconducting and a normal-metal at opposite sites. In a superconductor the current is carried by Cooper pairs which leads to the existence of a superconducting energy gap in the electron energy levels, thus tunneling is not the same as in the normal state. The energy gap on the superconductive electrode prevents low energy tunneling ($E < \Delta$), thus only electrons at the tail of Fermi distribution are able to tunnel to the other side (using low bias voltage). The tunneling current in a NIS junction has been found to be very sensitive to temperature, and can operate as a thermometer for sub-kelvin temperatures [13]. The NIS junction can also operate as an electron cooler, since only the hottest electrons from normal metal site are tunneled to the superconducting site.

2.2.2 Coulomb blockade

Electricity is the movement of electrons, and an ultimate goal is to manage electronics by controlling only a single electron. In 1987, the first single electron transistor was fabricated in Bell Laboratories [17].

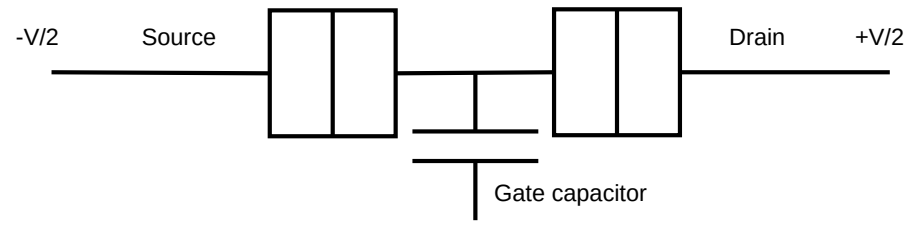

Figure 2.2: Schematic diagram of a single electron transistor, which is an application of coulomb blockade in a sample with two tunnel junctions in series. The potential of the island is controlled via a gate electrode.

Single electron transistor (SET) is constructed by connecting two tunnel junctions in series and by mounting a gate electrode in close proximity of the island (see Fig. 2.2). The operation principle is that the two tunnel junctions separate a small island where one extra electron can be confined. Electrostatics can dictate that the electron is not able to tunnel out from the island, unless the gate voltage has particular values. The electron movement can thus be controlled via the gate voltage, just like in an ordinary field effect transistors [18].

In this circuit the total capacitance of the island is

$$C_T = 2C_J + C_G + C_0, \tag{2.8}$$

where C_J is capacitance of the tunnel junction, C_G is the gate capacitance and C_0 is capacitance to ground and its charging energy for one electron is

$$E_c = \frac{e^2}{2C_T}. \tag{2.9}$$

Without a gate voltage, the island can only be charged with voltage $V > e/2C_T$ [18]. At voltages below this limit the conductance is suppressed, which is called a coulomb blockade i.e. the incoming electron has not enough energy to overcome coulomb repulsion. Of course, thermal energies must also be taken account: at high temperatures electron easily has thermal energy above the charging energy and no blockade is accomplished. The trick to operate SET at higher temperatures is to have a smaller junction area to maximize the charging energy. The repulsive coulomb force is more effective in smaller dimensions, thus a typical 100 nm $\times$ 100 nm aluminum island can only operated as a SET at very low temperatures where thermal energies do not dominate over the charging energy.

For room temperature operation, the single electron charging energy of the island, $E_C = e^2/2C_T$, must be large compared to the thermal energy $k_BT \approx 26$ meV (k_B is Boltzmann's constant and temperature $T = 300\,\mathrm{K}$). Therefore, the value of the C_T must be ≈ 1 aF or less, and in practice this implies that the charging island must be <10 nm in size [18].

Because of temperature dependence, this phenomenon can also be used in an application called coulomb blockade thermometer [19], which is an absolute thermometer for low temperatures (for temperatures obeying $E_C \ll k_BT$).

By studying the conductance as a function of bias voltage one can determine the full width at half minimum $V_{1/2}$ and the drop in conductance $\Delta G/G_T$ (see Fig. 2.3).

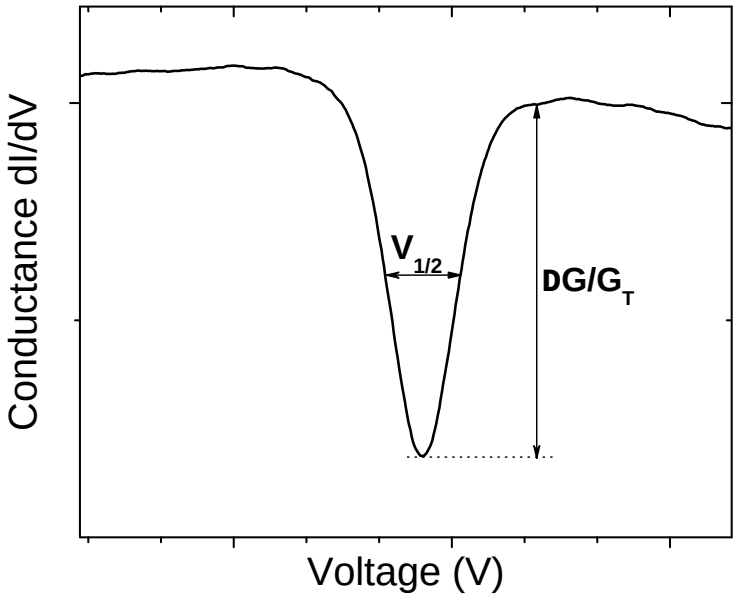

Figure 2.3: Full width at half minimum $V_{1/2}$ and the drop in conductance $\Delta G/G_T$.

For a symmetric double junctions array the relation is [20]

$$\frac{eV_{1/2}}{2k_BT} = 5.439, \tag{2.10}$$

from the temperature is determined straightforwardly, since the relation depends only on temperature. Thus, CBT is primary thermometer.

Also the relative dip-depth $\Delta G/G_T$ may be determined. This information can be used to calculate charging energies. For example, again for a double junction

array, the relation is as follows [20]:

$$E_c = 6k_B T \frac{\Delta G}{G_T}. \tag{2.11}$$

2.2.3 Quantum computation

A quantum computer is a device for computation that uses quantum mechanical phenomena, e.g. superposition and entanglement, to perform operations on data much faster than its classical counterpart does. A traditional computer operates using bits as a data while a quantum computer uses quantum bits, qubits, which are a superposition state i.e. containing all values of data simultaneously. The possibility for an unparalleled calculation speed for certain application originates from the simultaneous processing of the data in a qubit register.

Two-state quantum mechanical system can operate as a qubit if it satisfies some conditions e.g. it must not dissipate power and the temperature of the system must be much lower than the energy quantum associated with the transition between the states. So the coherent state of the qubit must not interact with outside universe as the slightest interaction with the external world would cause decoherence to the system. Different schemes have been developed to realize qubit, however in this project the solid state physics point of view was centre of attraction.

Superconductive circuits with tunnel junctions are a promising method to realize a SQUBIT (superconductive qubit) because to operate as a qubit the circuit must contain a non-linear component which tunnel junction is. The simplest circuit that contains a Josephson junction squbit is so called cooper pair box, which operates as a superconducting charge squbit (SCQ), i.e. a Cooper pair box [21], which is biased so that only two nearby charge states are accessible, e.g. zero and one extra Cooper pair in the box.

Fig. 2.4 shows a schematic diagram of a Josephson charge qubit, where $\pm Q_j$ denotes charges induced at the electrodes of the Josephson junction with the capacitance C_j and the Josephson energy E_j , while $\pm Q_g$ denotes charges induced at the electrodes of the gate capacitor C_g. The circuit is biased by the voltage V_g. The part enclosed by a broken line comprises the Cooper pair island whose excess

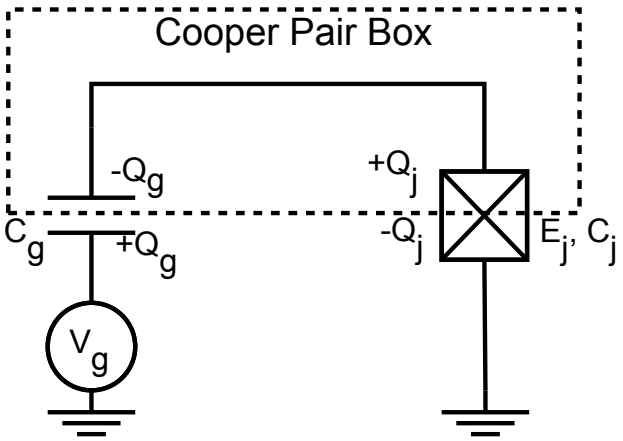

Figure 2.4: Schematic diagram of a Josephson charge qubit.

charge (in units of $2e$) corresponds to the qubit degree of freedom [22].

Since the single electron transistor (SET) is an extremely sensitive charge measurement device it is an obvious candidate as read-out device for solid state charge qubits [23].

Quantum computation relies on the coherence of the system, so qubits must have long enough dephasing time to process calculations. Decoherence due to interaction from the outside universe eventually causes superposition to collapse with some dephasing time.

Different methods for decoherence exists e.g. Josephson energy fluctuates in time because of imperfections in barrier, which also influences on qubit potential energy [3]. These resistance fluctuations are seen in 1/f noise figures. The 1/f noise may emerge from the substrate or tunneling barrier, thus by decreasing the 1/f noise the qubit decoherence will be decreased.

Chapter 3

Experimental procedures and results

3.1 Sample fabrication

Several Al–AlO_x–Al tunnel junctions were fabricated using conventional electron beam lithography and a vacuum shadow evaporation techniques, where the metal deposition takes place at different angles. The schematic idea of the procedure is illustrated in Fig. 3.1 and the SEM image of an actual junction is in Fig. 3.2.

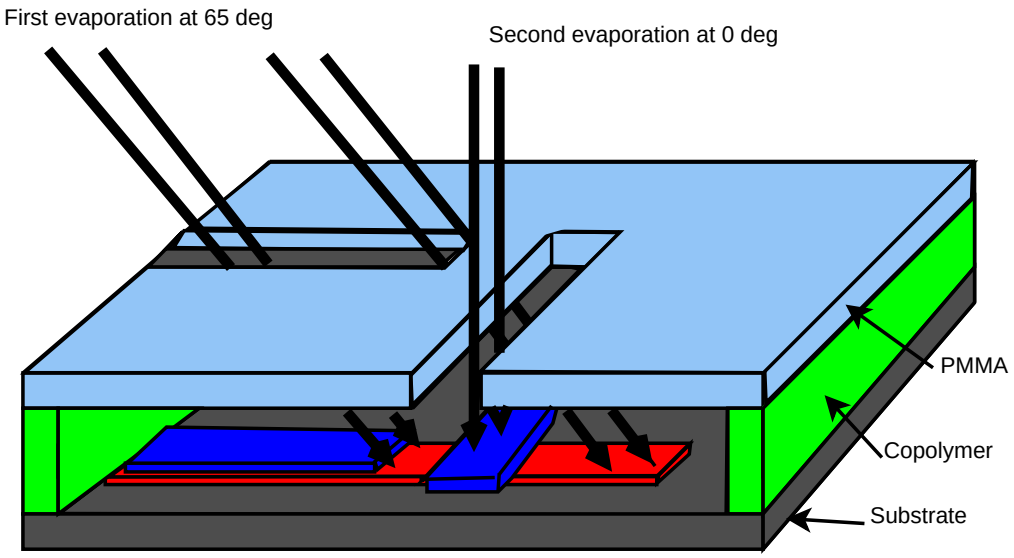

Figure 3.1: Schematic picture of a shadow evaporation technique. Resist coated chip has so called undercut structure (the hollow area). Metal deposition is done twice, at first from 65°angle and secondly at zero angle. After depositions, the aluminum is oxidized.

The substrate, silicon chip, is at first coated by two resist layers that dissolve in developer at the regions exposed to electron beam. The lower resist layer dis-

solves more than the upper one leading to a hollow area underneath the upper resist layer, which operates as a screen while evaporating metal onto the chip.

The first evaporation at angle of $\approx 65^\circ$ deposits thin metal film onto the red-colored region in Fig. 3.1. The cap in the upper layer shadows the area at the second evaporation at angle of 0° thus separates the topmost metal film (blue) to conduct only through the lower layer (red). Between the metal layers, the dielectric oxide operates as a tunneling barrier. The oxide is grown thermally (at room temperature) between the separate aluminum depositions.

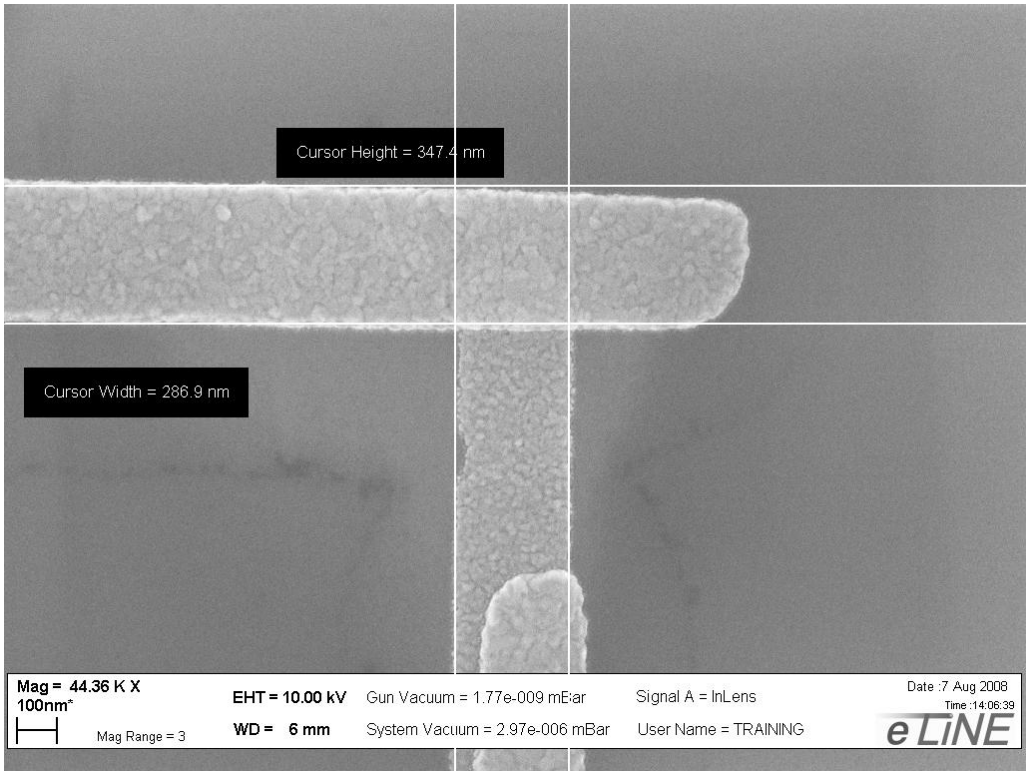

Figure 3.2: Scanning electron microscope image of a tunnel junction. Line widths are approximately 300 nm each.

The junction geometry was unchanged for every sample, but the substrate and the evaporator were different. The two different substrates used were nitridized and oxidized silicon wafers. The SiN was grown by LPCVD at UC-Berkeley Microfabrication Laboratory to a thickness of 300 nm and the SiO was thermally oxidized here at NSC to a similar thickness. The substrates are referred as SiN and SiO, respectively. Before metal deposition, the chip was cleaned with O_2 plasma at 30 W power in a reactive ion etcher with pressure of 40 mtorr and 50 sccm flow.

The most of the samples were fabricated in ultra high vacuum (UHV) while other part in high vacuum (HV). The Balzers HV evaporator has no loading

chamber and achieved only a high vacuum of $\sim 10^{-6}$ mbar. The UHV evaporator has a separate loading chamber, while the evaporation chamber is kept at ultra high vacuum of $\sim 10^{-8}$ mbar

The thickness of the first metal layer was about 50 nm and the second about 100 nm. Oxidation differs between the two evaporators. For HV evaporator it was done at 10 mbar pressure for 4 minutes and for UHV at 200 mbar for 5 minutes. With such a settings, the UHV fabricated samples had tunneling resistances of about 10–20 kΩ, while for HV fabricated samples the tunneling resistances were about 3–4 times greater. Line widths were evaporator independent, so the only variable causing the difference in resistance was the barrier properties, i.e. oxidation and cleanliness. Substrate has no direct effect on tunneling resistance, nor were any other differences between the different substrates detected. After deposition, the adsorption of the moisture was minimized by post-oxidation. The line widths of measured samples were about 300–400 nm, thus the junction area size is about 0.1 $\mu\mathrm{m}^2$. Deposition rate of Al was about 0.1–0.2 nm/s to have a better uniformity.

3.2 Annealing

Tunnel junctions are not necessarily stable, which hinders the applications that require junctions to be stable in time. The oxide barrier has imperfect crystal structure after fabrication, thus the barrier atoms may try to spontaneously reorganize to equilibrium positions. This is seen as an increase of tunneling resistance with time. At room temperature, this spontaneous relaxation takes a long time. Also, one possible explanation might be that the barrier absorbs other unwanted molecules inside to fill vacancies, since vacuum conditions prevent aging significantly [24].

The trick to stabilize junctions is thermal annealing. In that process a high temperature furnace, placed in vacuum, is used for rapid heating of the sample. Slow cool down is achieved via a sample stage with a low thermal conductance and enough heat capacity. In our oven, the surface of the sample stage is made out of a ~ 1 mm thick copper plate while the supporting structure is ceramic. Via slow cool down, the barrier structure will relax more likely into a minimal energy

configuration i.e. into a well organized lattice structure.

The annealing procedure was at first to heat up the furnace to the set point temperature, and to let it stabilize with no sample inside. When warmed up, the sample was injected into the tubular furnace and allowed to warm while monitoring the temperature of the sample stage. Immediately after the designated temperature was reached, the sample was pulled out of the furnace. Achieved characteristic temperature by time diagrams are illustrated in Fig. 3.3, where the target temperature of the sample stage was always 400 centigrades while furnace temperature was altered.

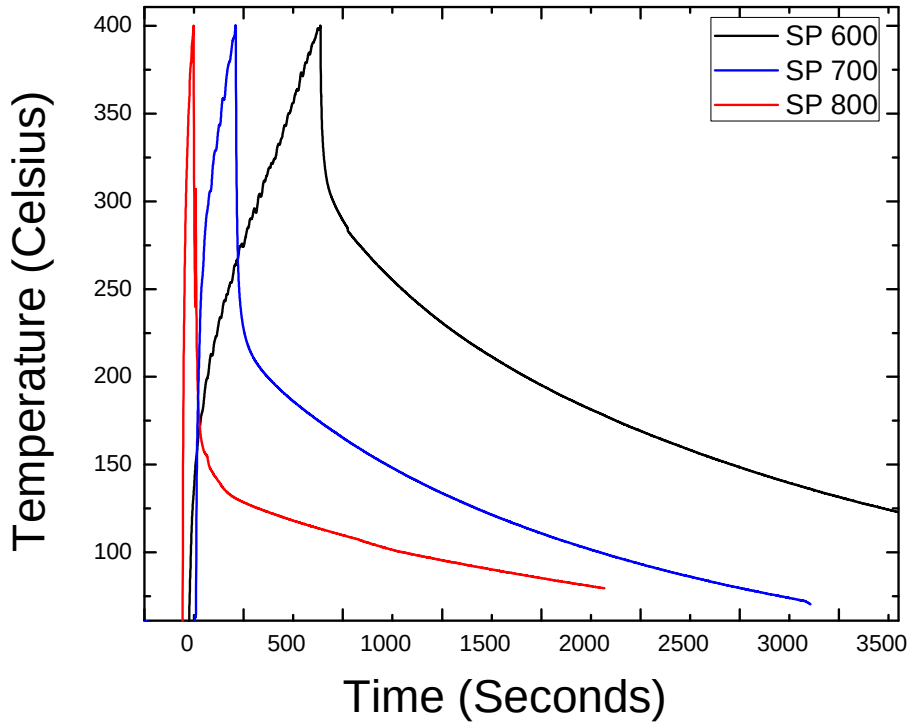

Figure 3.3: Heating and cooling diagrams of the annealing process using different set point temperatures (SP 600, 700 and 800 °C). In all cases the sample stage was heated to 400 °C. Higher temperature means both faster warming and cooling down because the whole sample stage has not enough time to warm up completely. The temperature is measured on the surface of the sample stage using a thermocouple.

For a slow cool down but with still a reasonable heating time, the furnace temperature of 600 °C was chosen. The maximum annealing temperature the samples survived was found to be around 400 °C. By such an annealing recipe, the samples stabilize very well. It agrees with previous results [4], where samples fabricated in HV evaporator (Balzers) were studied.

Aging was also detected in UHV fabricated samples, although they age much less than the HV fabricated samples. It is obvious that the HV fabricated samples are inferior, since they are fabricated in dirtier conditions, so that the increase in resistance is much faster than in samples fabricated in UHV.

Annealing at 400 °C stabilizes both junctions. Tunneling resistances increased about 10–45% for UHV fabricated samples and 200–300% for HV fabricated samples. The early annealings for HV fabricated samples led to an increase of about 1000% (initially resistances were couple of dozen kilo ohms), but reduced to traditional levels after cleaning the evaporation chamber. Probably it was due to a contamination of the HV chamber.

3.3 Conductance measurements

Conductance as a function of voltage gives significant information on the structure of junctions. The spectrum can be used to interpret the barrier properties, e.g. resonance peaks are usually caused by unwanted impurities (charge traps) within the barrier, while the conductance of a perfect barrier should be parabolic (see Eq. 2.7).

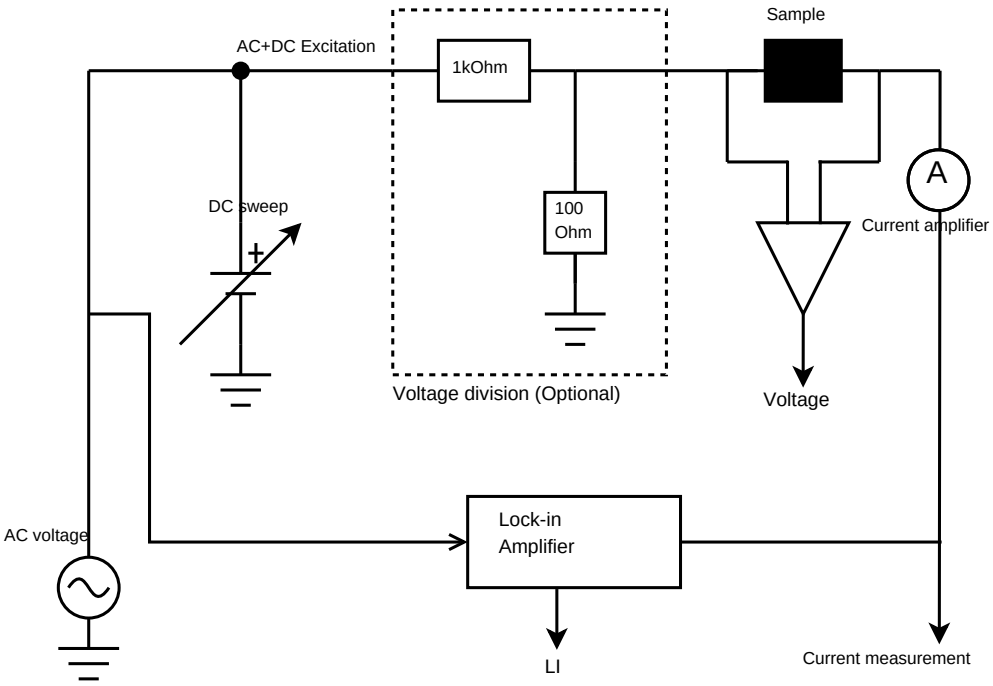

Figure 3.4: Conductance measurement using lock-in amplifier.

Conductance was measured using a lock-in-amplifier setup illustrated in Fig.

3.4. The current through the sample contains an oscillating AC signal and DC bias, the total current is in the first order approximation

$$I \approx I(DC) + \frac{dI}{dV}(V_{DC})V_{exc}\sin(\omega t). \tag{3.1}$$

The current is converted to voltage in the current amplifier and then fed into the lock-in amplifier.

Lock-in amplifier detects the coefficient of the first harmonic of the signal supplied in i.e. $\frac{dI}{dV}(V_{DC})V_{exc}$, which is in the root-mean-square voltage units. Simultaneously the DC voltage over the sample was measured. From the measured data pairs, lock-in signal and excitation voltage, the conductance can be calculated.

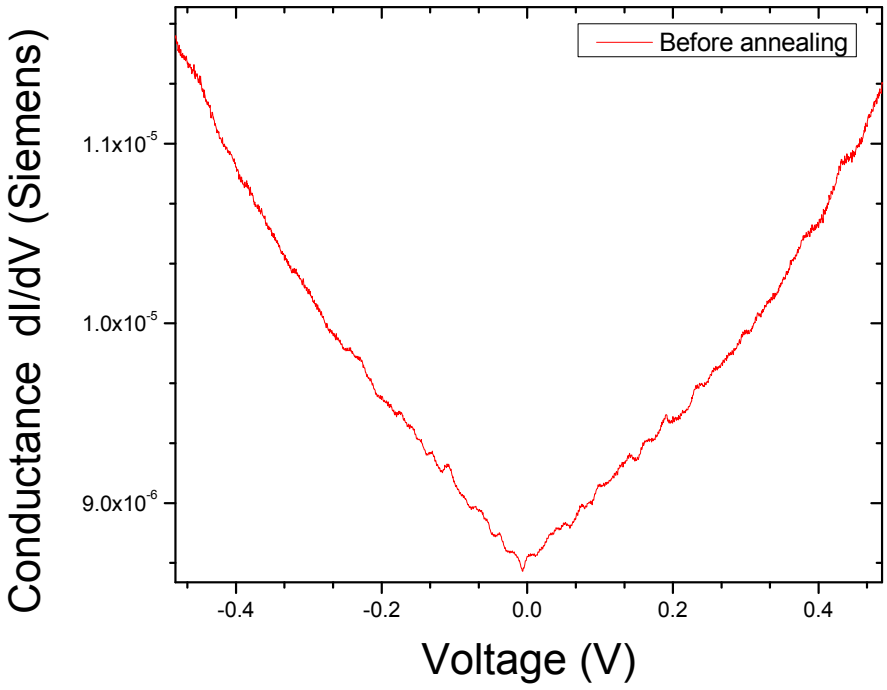

Figure 3.5: Conductance spectrum of 110.5 kΩ HV fabricated sample at liquid helium (4.2 K).

HV fabricated samples produce initially quite peaky spectrum (see Fig. 3.5), which can be improved by annealing [4]. Meanwhile, as predicted, samples fabricated in UHV possess more parabolic spectra that annealing does not change much (see Fig. 3.6).

Interesting detail was the discovery of Coulomb blockade (Section. 2.2.2) in single junction samples (see Fig. 3.7). Coulomb blockade was found in every sample, and remained even without the typical double-junction geometry. The

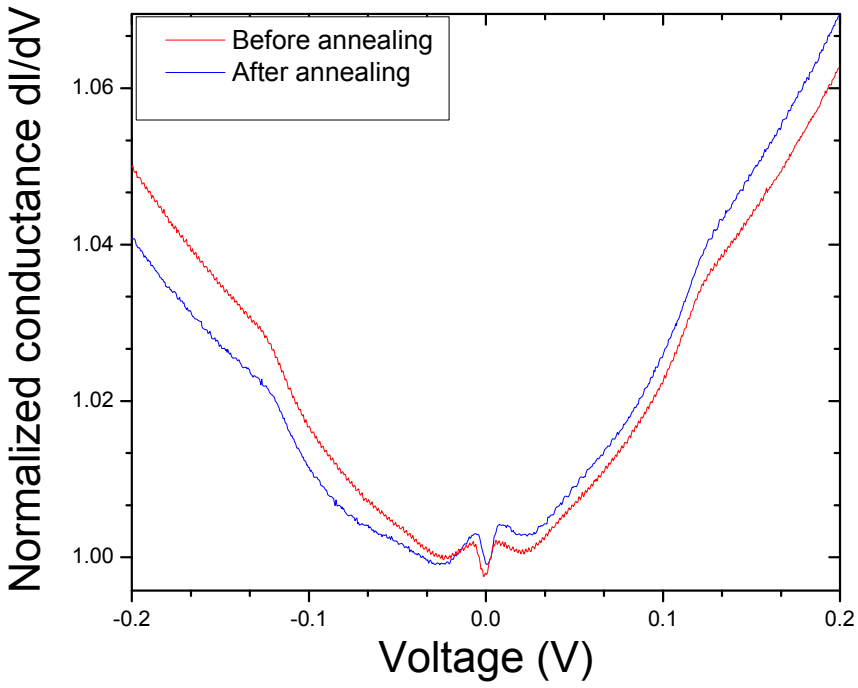

Figure 3.6: Normalized conductance spectra of UHV fabricated sample at liquid helium (4.2 K) before (red) and after (blue) annealing, where conductance is normalized by zero bias conductance.

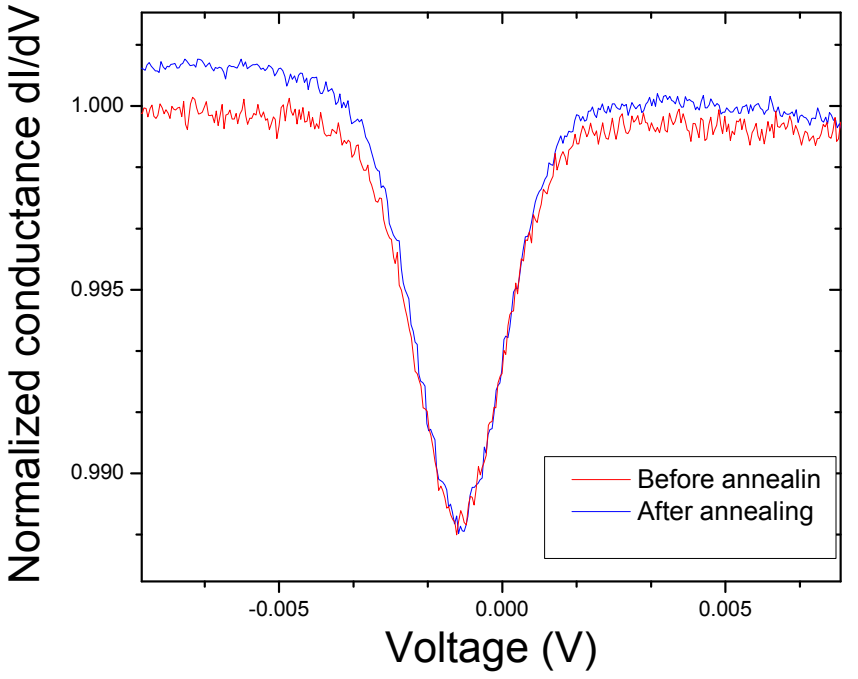

Figure 3.7: Normalized conductance spectra of UHV fabricated sample at liquid helium (4.2 K) before (red) and after (blue) annealing in the coulomb blockade region where conductance is normalized by the background level.

actual source of the phenomenon was left unknown though it might be due to influence of the circuit resistance.

3.4 Noise measurements

In this section, different noise measurement setups are described. Measuring of noise requires a sensitive technique since tunnel junctions are destroyed by large currents and background noise needs to be eliminated.

The different measurement setups have always in common the same type of lock-in amplifiers (Stanford Research Systems SR830) and the spectrum analyzer (Agilent 89410A) to measure noise in units of power spectrum V^2/Hz. Two different types of low noise voltage preamplifiers were used, PerkinElmer 5184 [25] and Ithaco 1201 [26]. As will be discovered, the preamplifier noise is the most limiting factor in the measurement setup and it must be get rid of.

The Fourier transform that the spectrum analyzer performs, was done using the "Hanning" window since it has the lowest noise floor, with moderate amplitude accuracy and frequency selectivity. It could have been imperfect choice since the 1/f-noise measurement requires mostly high amplitude selectivity, which "Flat-top" windowing possesses. However, the difference between these two modes was experimentally found to be insignificant.

In the measurement setup, the source of the measured noise must be confirmed to emerge from the sample, not from other parts of the circuit, e.g. from preamplifiers. This test was carried out by measuring noise figures of typical 1 $\mathrm{k}\Omega$ resistors, which possess low Johnson noise without significant $1/\mathrm{f}$ noise, and by comparing the results to theoretically estimated Johnson noise levels.

3.4.1 Single amplifier noise measurement setup

The simplest method to measure noise is to measure voltage fluctuations without current bias, although in the absence of current bias there is no $1/\mathrm{f}$ noise present, i.e. Johnson noise is only detectable.

The measurement setup is illustrated in Fig. 3.8, which simply measures voltage over the sample. The voltage is amplified in the preamplifier and the ampli-

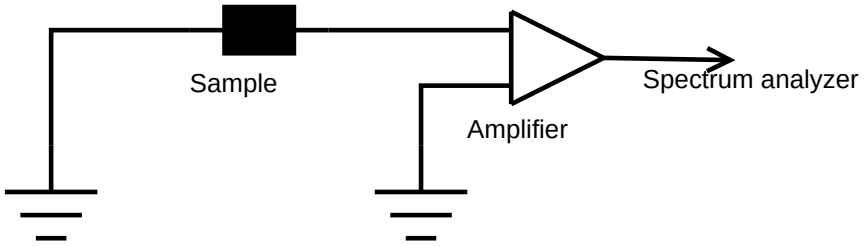

Figure 3.8: Single amplifier noise measurement setup.

fied signal is fed into the spectrum analyzer.

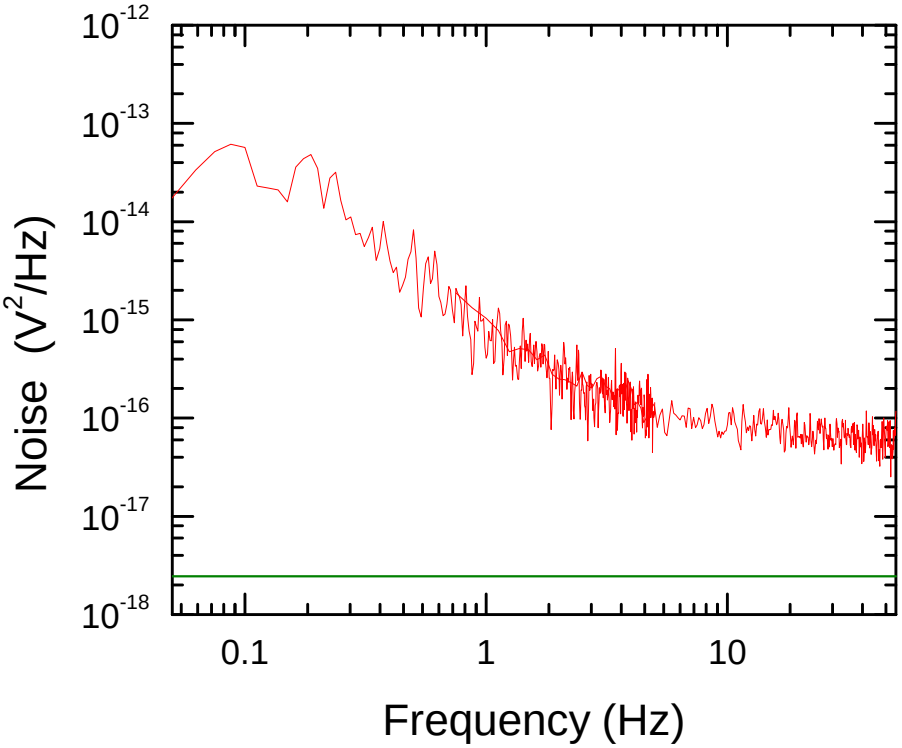

Figure 3.9: Noise spectrum of 10 kΩ tunnel junction at 4.2 K using PerkinElmer preamplifiers in single amplifier setup. The horizontal line is theoretically estimated level of Johnson noise.

The noise spectrum of 10 kΩ tunnel junction at 4.2 K using PerkinElmer preamplifier is shown in Fig. 3.9. It shows the 1/f segment below 10 Hz frequencies and after that, it saturates to the white noise level. Unfortunately, the measured white noise is much higher than the expected Johnson noise illustrated as the horizontal line. In addition, the 1/f noise should not be present, since no current is driven through the sample. Thus, the noise measured is mostly coming from somewhere else than from the sample, possibly from the preamplifier.

The noise floor can be estimated by measuring the noise level with amplifier input shorted. The result is in Fig. 3.10 and matches precisely to Fig. 3.9. The

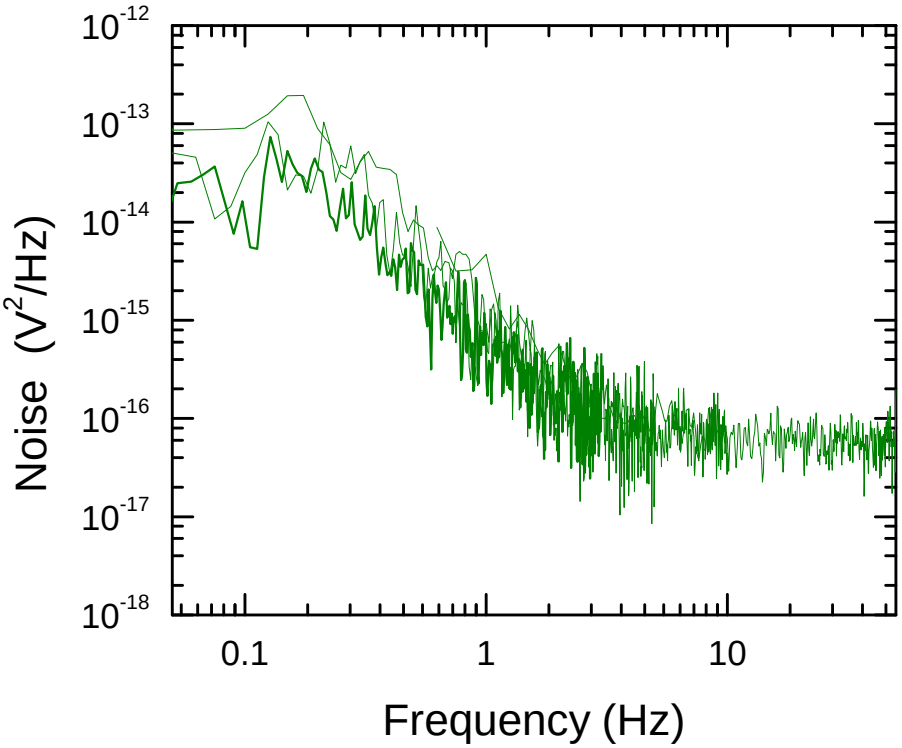

Figure 3.10: The noise floor of the setup where preamplifier inputs were short circuited.

conclusion is that with this setup only noise of very high resistance samples or at high temperature (high Johnson noise level) can be measured since low noise levels are suppressed by preamplifier noise.

3.4.2 Cross-correlation technique

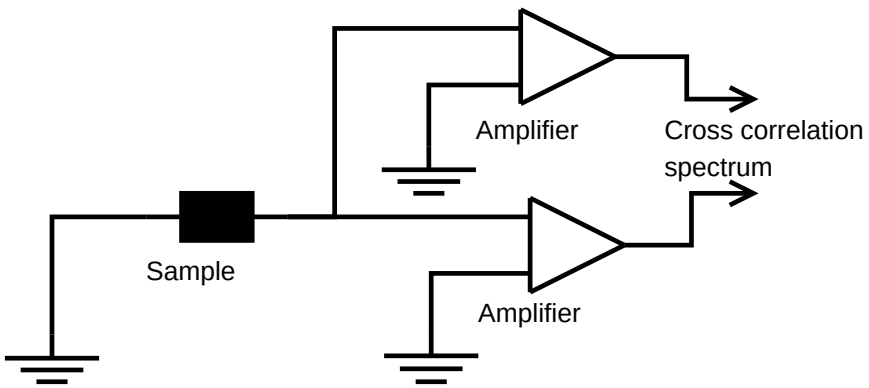

Figure 3.11: Double amplifier cross-correlation setup.

The next step to improve noise measurement setup is to use two preamplifiers and to measure only correlated components of these two signals. The spectrum

analyzer has a built in cross-correlation feature, which can be used to reduce contact and preamplifier noises [27]. The operational principle is to gather data in time domain, i.e. phase sensitively, and to multiply the two signals. Then only signals with the same phase are taken into account. Thus, the technique basically measures only correlated signals coming from sample while, rejecting uncorrelated signals from cables and preamplifiers.

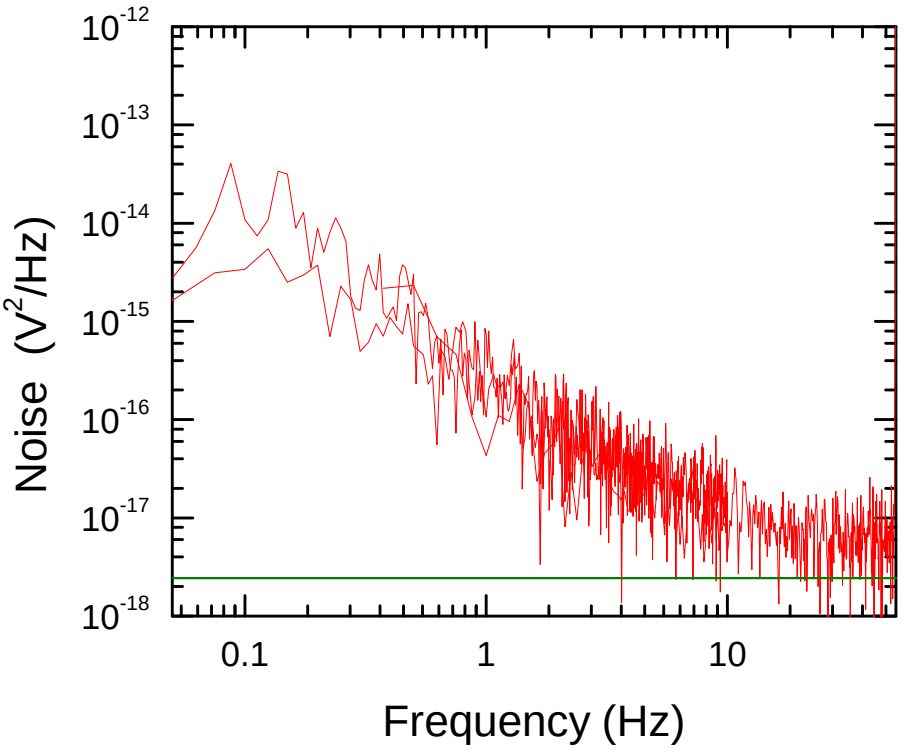

Figure 3.12: Cross-correlation noise spectrum of 10 kΩ tunnel junction at 4.2 K using two PerkinElmer preamplifiers. The horizontal line is theoretically estimated level of Johnson noise.

The measurement results are in Figs. 3.12, 3.13, 3.14 where substantial noise level drop down to the theoretical Johnson noise estimate was found. Therefore, this method very effectively reduces the white noise level at higher frequencies, while the low frequency spectrum still possesses a high $1/f$ spectrum. As before, the baseline check was carried out, which revealed that the measured noise was again pure preamplifier noise dominated by the $1/f$ part at low frequencies and a white noise level, which by chance saturated close to the Johnson noise level of the sample. Thus, the minimal noise level this setup can measure is at the level of

$$S_V = 4k_B \cdot 4.2K \cdot 10 \cdot 10^3\Omega \approx 10^{-18}\mathrm{V}^2/\mathrm{Hz}. \tag{3.2}$$

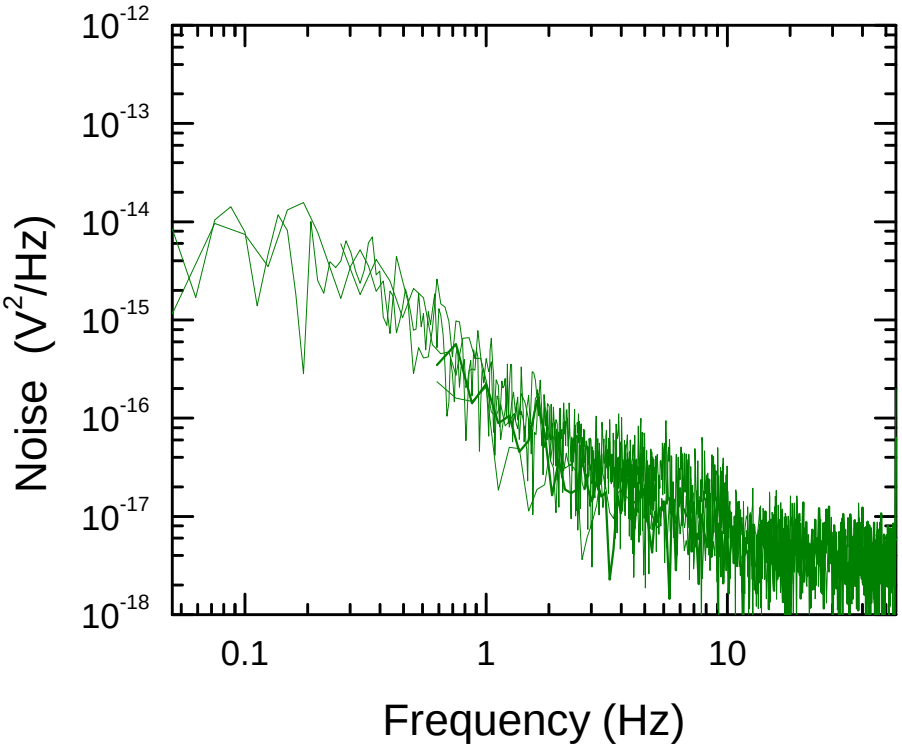

Figure 3.13: Noise floor of the cross-correlatíon setup using two PerkinElmer preamplifiers.

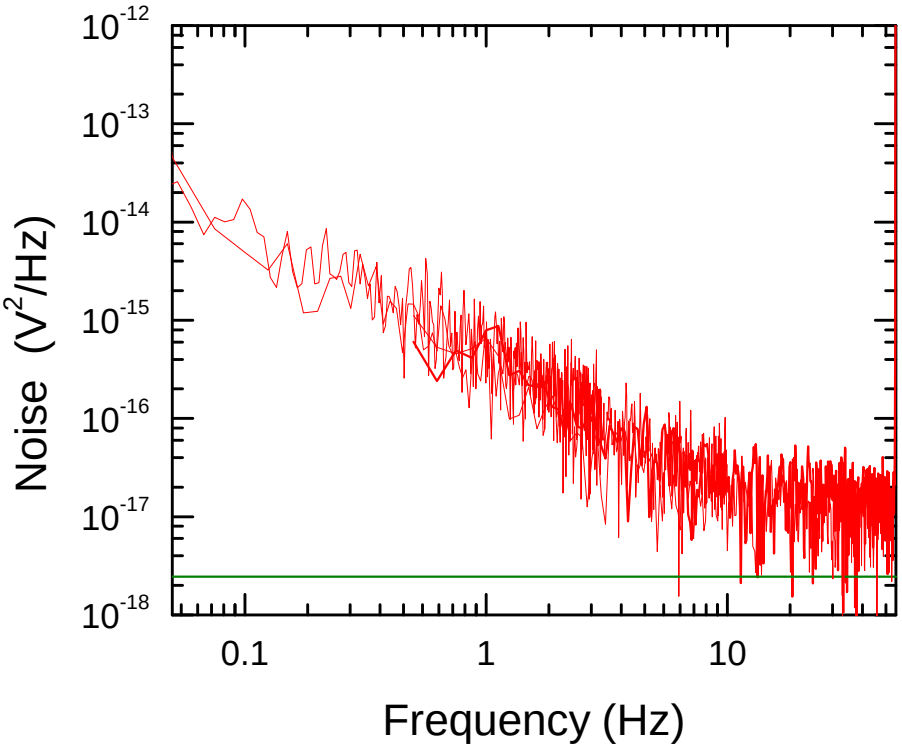

Figure 3.14: Cross-correlation noise spectrum of 10 kΩ tunnel junction at 4.2 K using Ithaco 1201 preamplifiers. The horizontal line is theoretically estimated level of Johnson noise.

The same measurement was carried out by using Ithaco preamplifiers. The result is shown in Fig. 3.14. It is almost the same as for PerkinElmer preamplifiers, but a slight increase in noise level overall. That is predicted, since the manuals tell that Ithaco preamplifiers have a higher noise level than the PerkinElmer preamplifiers [25], [26].

3.4.3 Bridge measurement setup

All these previous methods lack the driving current through the sample, thus preventing 1/f noise measurement since it emerges from resistance fluctuations. They work fine for Johnson noise measurements at frequencies higher than 10 Hz, but it is impossible to measure anything else. The next step is to apply current and measure voltage differences caused by driven current. Direct four terminal noise measurements (see Fig. 3.15) over a sample would not be feasible since the voltage drop over a sample would be much higher than the weak noise signal, thus overloading the input of the spectrum analyzer. What is needed is a way to subtract the DC voltage from the signal before feeding into preamplifiers. The balanced bridge circuit in Fig. 3.16 accomplishes the task. The variable ballast resistor is used to balance the bridge i.e. the amplifier sees no DC voltage. The noise measured is coming from both samples in series.

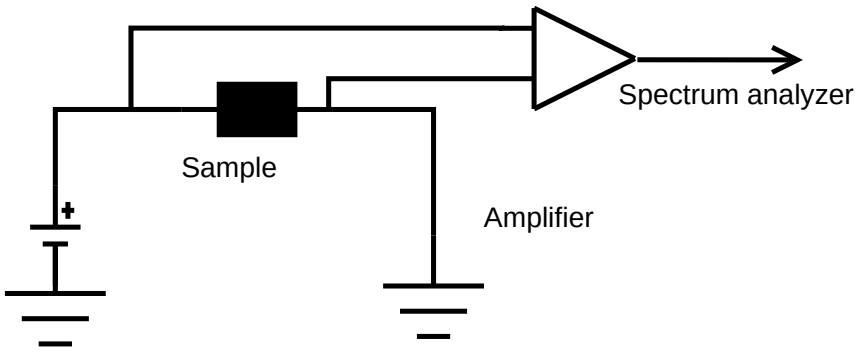

Figure 3.15: Simple DC noise measurement.

3.4.4 AC bridge measurement setup

DC bridge circuit still has the serious drawback that the high low frequency 1/f preamplifier noise dominates the noise spectrum. As before, the cross-correlation

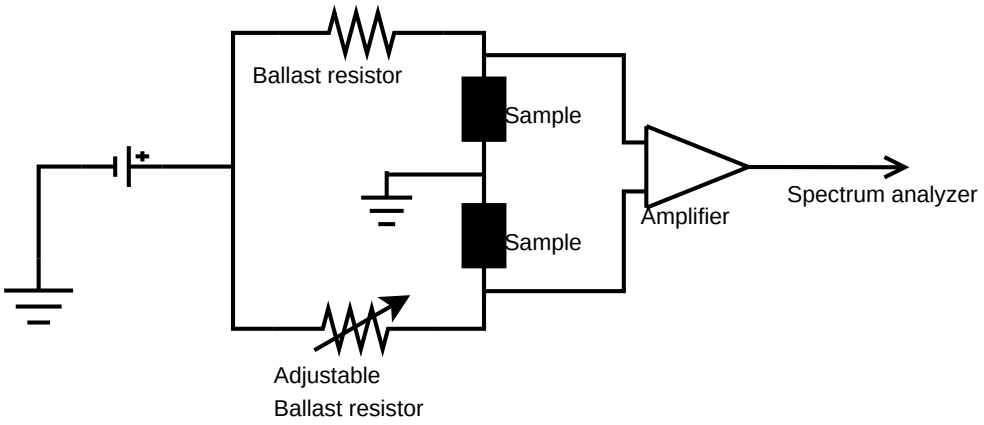

Figure 3.16: Balanced DC bridge where DC part is subtracted away.

via two preamplifiers can be used to reduce noise. The usage of cross-correlation provided a huge improvement in noise floor, but the high 1/f noise from preamplifiers still remains. The method to overcome this limitation is to "shift" the measurement into the lowest noise frequency region of the preamplifiers, which is determined from the preamplifier data sheets [25], [26]. The frequency shift is done by using an AC bridge modulation technique [28] where the sinusoidal excitation signal is used to drive the bridge circuit, and a lock-in amplifier to detect and demodulate the noise (see Fig. 3.17). The excitation frequency is chosen to match the optimum low-noise frequency of preamplifiers.

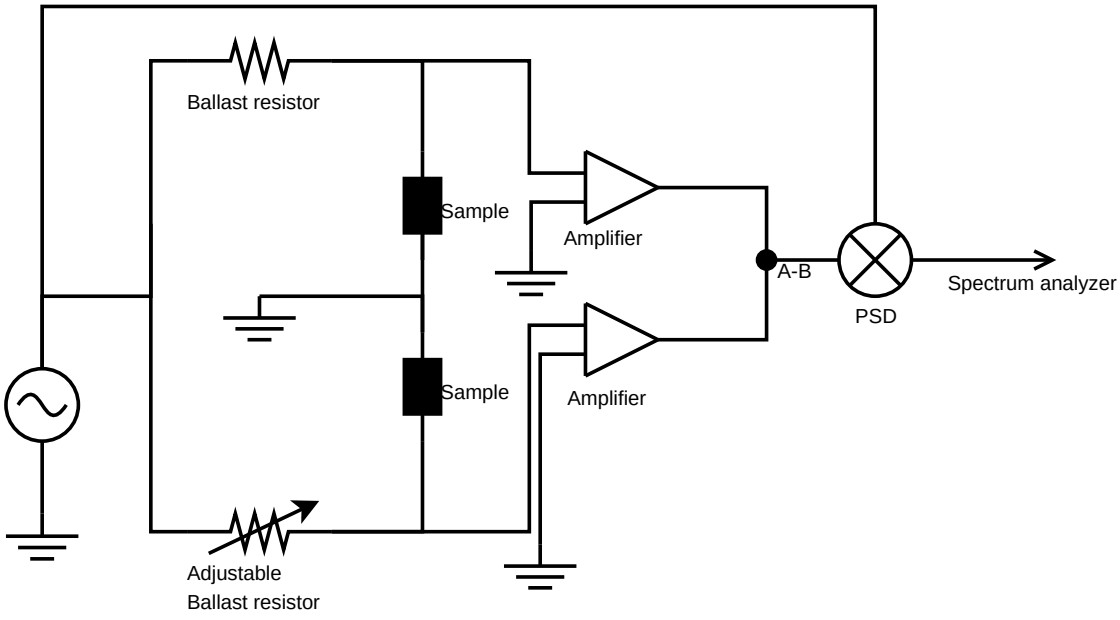

Figure 3.17: AC Bridge measurement using two PerkinElmer preamplifiers to function as a single differential amplifier. As an alternative, one true differential preamplifier can be used to replace these two semi differential preamplifiers.

The circuit operates much like an AM radio. The constant amplitude and frequency sine wave (carrier signal) is fed through the samples, whose resistance noise modulates the amplitude of the incoming sine wave. The ballast resistors are large compared to the sample resistance, thus the current through the circuit can be considered to be constant. The fixed ballast is a 1 MΩ low noise wire-wound resistor, in comparison to a sample resistance of 100 kΩ, at maximum. The adjustable ballast resistor is a precision resistance decade box made out of low noise resistors. Also, the balanced bridge subtracts the excitation, thus the voltage fluctuation measured over the tunnel junctions are emerging only from the noise. The lock-in amplifier demodulates this noise by multiplying the output signal by the reference channel (PSD detection) and outputting a more slowly varying voltage, which can then be analyzed.

The lock-in is used since it can detect the phase of the signal. The noise fed to the circuit has initially a zero phase shift but the modulated signal coming from the setup can be shifted by some arbitrary phase depending on the capacitive and inductive properties of the system. The noise from the sample appears at the in-phase component of the signal while all other noises have random phases and are rejected by the lock-in amplifier [28].

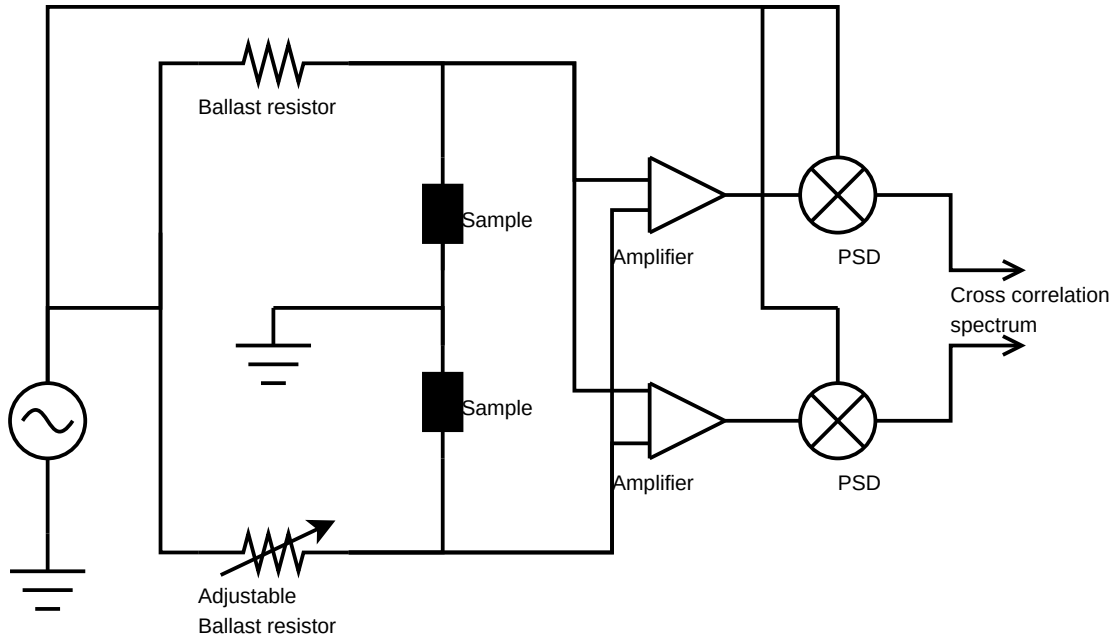

Figure 3.18: AC modulation bridge noise measurement setup with two lock-in amplifiers and cross-correlation spectrum analyzing. Here two differential preamplifiers are used. The fixed ballast resistor is a low noise wire wound resistor with resistance of 1 MΩ. The adjustable resistor is used to balance the bridge.

This setup disposes the problem of high 1/f noise of preamplifiers. Now the limiting factor is the preamplifier noise at the excitation frequency. Once more, the cross-correlation technique is applied (see Fig. 3.18) to reduce overall noise floor. Two preamplifiers and two lock-in amplifiers at the same reference signal are used. Since this circuit is biased, the preamplifiers must have full differential inputs that are absent in PerkinElmer preamplifiers, so in the results shown later only Ithaco preamplifiers were used, although they possess a higher noise level.

Phase sensitive detection is itself quite effective, so the cross-correlation has not such a great influence as it had in the case of unbiased noise measurement, but the change is still well noticeable. In Fig. 3.19 is measured noise of two 1 kΩ resistors at liquid helium using single lock-in versus double lock-in and cross-correlation. Theoretical Johnson noise estimate (horizontal line) is still unreached, but yet closer. Notice that the 1/f spectrum of preamplifiers seen in Figs. 3.9, 3.12 is totally gone. At room temperature, the noise of a similar 2 kΩ resistor can be measured accurately (see Fig. 3.20), where the measured noise level matches precisely with the theoretical Johnson noise level (horizontal line). Different excitation amplitudes had no effect on the noise spectrum; the 1/f spectrum was still missing. Several traditional carbon and surface-mount resistors were measured with no detectable 1/f noise.

Once again, this measurement confirms the noise floor is at maximum

$$S_V = 4k_B \cdot 300K \cdot 2 \cdot 10^3\Omega \approx 3 \cdot 10^{-17}V^2/Hz \tag{3.3}$$

for also lower frequencies. Real tunnel junctions posses resistances much greater than 2 kΩ, and since 1/f noise is always excess noise the measurements are accurate.

3.4.5 Frequency and phase dependence

The excitation frequency has always been set to about 1 kHz, which was check not to be cut off due to the time constant of the circuit. Some measurements were performed using variable excitation frequencies, and no significant changes were found. Fine-tuning the frequency may be used to reduce unwanted peaks in the noise spectrum, e.g. excitation should not match with the frequency of the mains

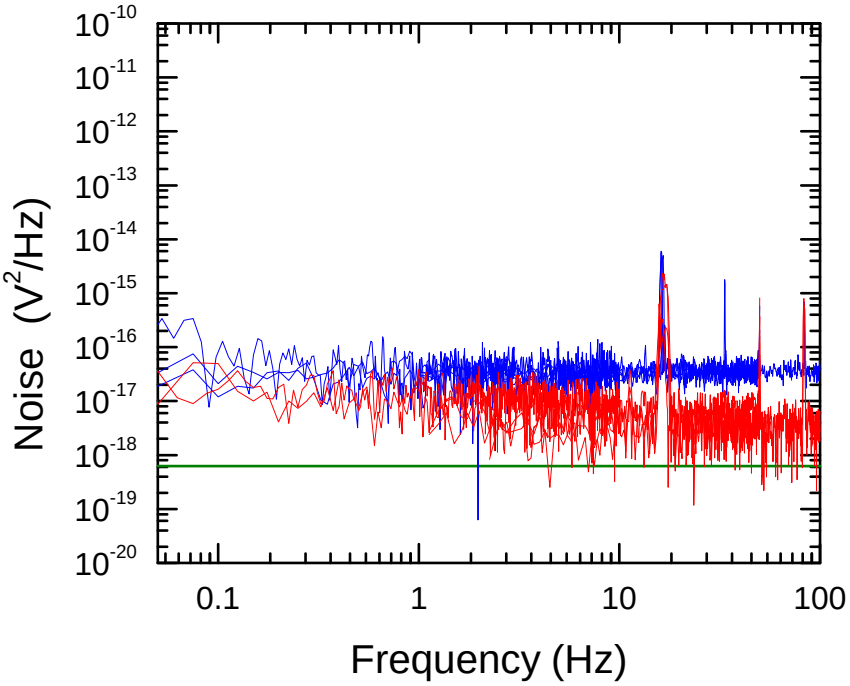

Figure 3.19: Noise figures of a 2 kΩ resistor at 4.2 K measured using the AC bridge circuit via single lock-in (blue) versus double preamplifiers with double lock-in cross-correlation setup (red).

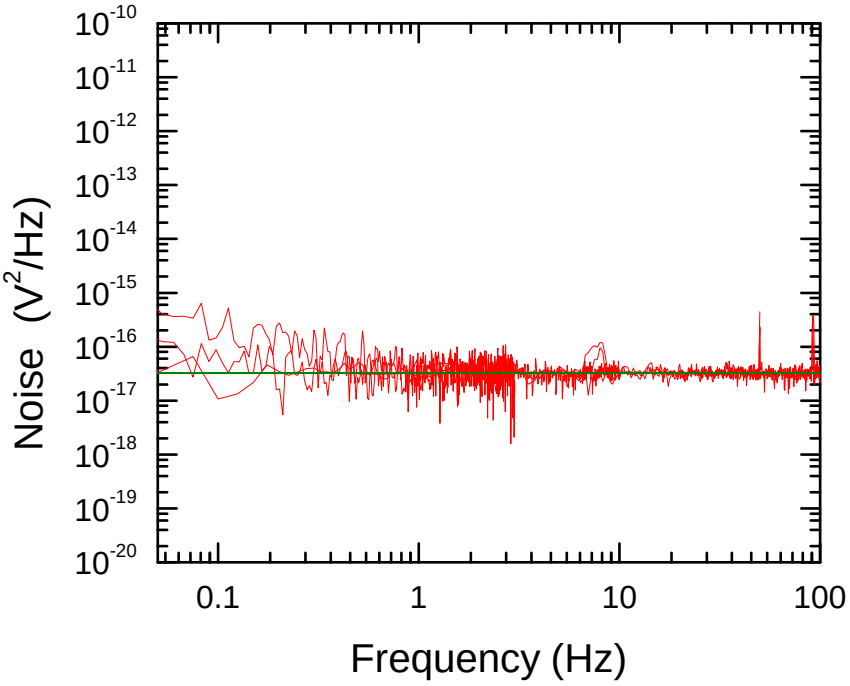

Figure 3.20: Noise figure of a 2 kΩ resistor at room temperature measured using the AC bridge circuit via double preamplifiers with double lock-in cross-correlation setup.

voltage (50 Hz) or its harmonics.

The phase shift through the circuit must be determined experimentally by measuring noise spectrum using detection at different phase shifts. The maximum noise level is achieved in-phase, while the lowest level is $\pm 90^\circ$ apart from it. The characteristic phase shift varies usually between $\pm 50^\circ$ from zero and, unfortunately, changes in every measurement because of the changes in the circuit e.g. in the ballast resistor box. Luckily, the precise noise shift is not needed to determine every time, since the maximum noise is achieved at rather high phase spread around maximum, as seen in Fig. 3.21.

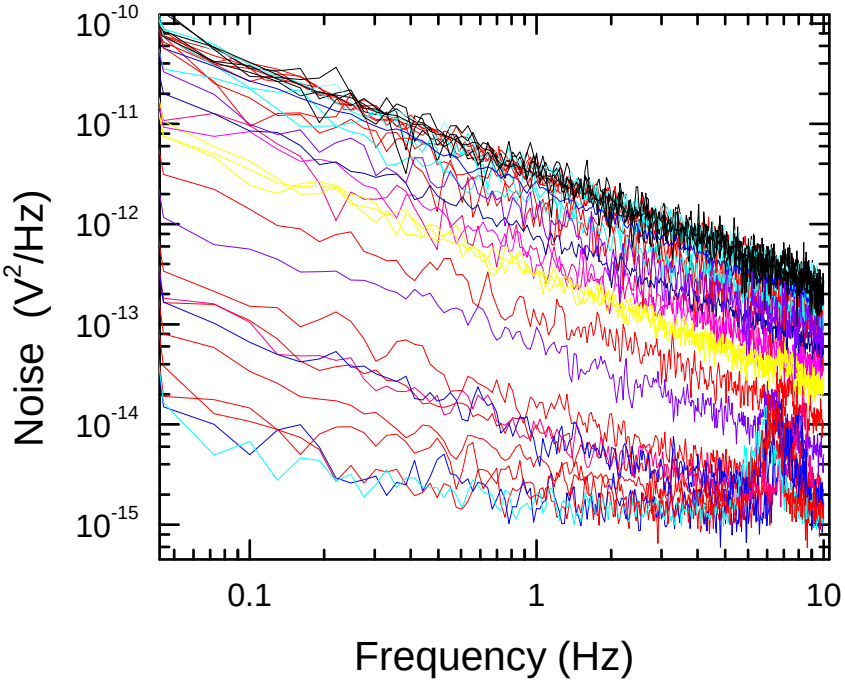

Figure 3.21: AC bridge noise measurement using double lock-in amplifiers and cross-correlation technique of tunnel junctions. Every curve represents noise spectrum captured using different phase selectivity. Thick black lines are at phase of 0° while the maximum level is not changing detectable at phase shifts below $\approx 30^\circ$. The noise floor is flattening rapidly while approaching the minimal off-phase which is at this case at $+72^\circ$. Bright yellow curves are at $\pm 90^\circ$ of phase. The maximal noise should be at -18° of phase ($+72^\circ - 90^\circ = -18^\circ$).

The noise minimum is always the Johnson noise level of the sample, since it does not depend on the phase. Search for the precise value of the phase shift requires fine-tuning in steps below one degree of phase, which was found to be too time consuming for every measurement. Thus, we rejected it, since it was already confirmed that the noise floor is at the Johnson noise level of the sample, and that the in-phase noise level is not so critical on the precise phase shift.

3.4.6 Noise in tunnel junctions

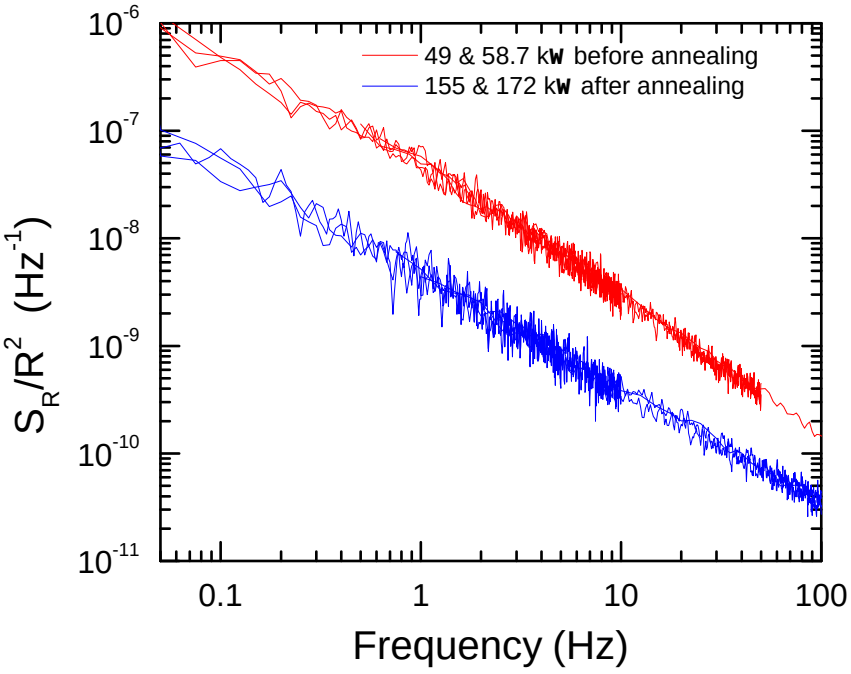

Figure 3.22: Double lock-in cross-correlation noise spectrum of tunnel junctions at room temperature. Samples were fabricated on SiO-chip in HV and annealed at 400°C.

The 1/f noise depends on excitation; with higher excitation amplitude, higher 1/f spectrum is achieved. Since tunnel junctions break down easily, low excitation voltages were used. Usually, the initial voltage from the oscillator was about 100 mV, which was raised up to 4 V, if needed. 100 mV excitation voltage from the oscillator corresponds about 100 nA current though the junction which leads to voltage difference over the junction (10 kΩ) to be about 1 mV.

Different excitation amplitudes lead to different voltage noise spectra. The bias current through the sample can be calculated, and then the voltage noise S_V converted to resistance noise S_R (see Eq. 2.3). Resistance noise can also be normalized by dividing by the sample resistance, thus providing a noise spectrum independent on both excitation and sample resistance.

The reduction of 1/f noise by annealing was found in every sample. In Figs. 3.22, 3.23 are junction pairs with different junction areas fabricated on the same SiO-chip in HV. They possess initially higher noise levels than samples evaporated in UHV, Fig. 3.26, but after annealing the noise levels drops approximately to the same level. The substrate was found to have no effect on the noise level,

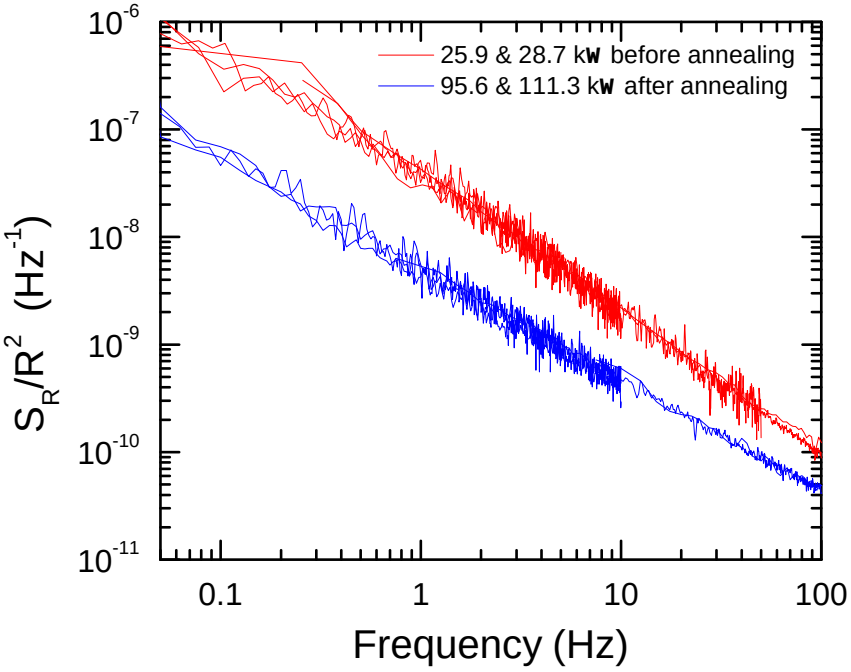

Figure 3.23: Double lock-in cross-correlation noise spectrum of tunnel junctions at room temperature. Samples were fabricated on SiO-chip in HV and annealed at 400°C.

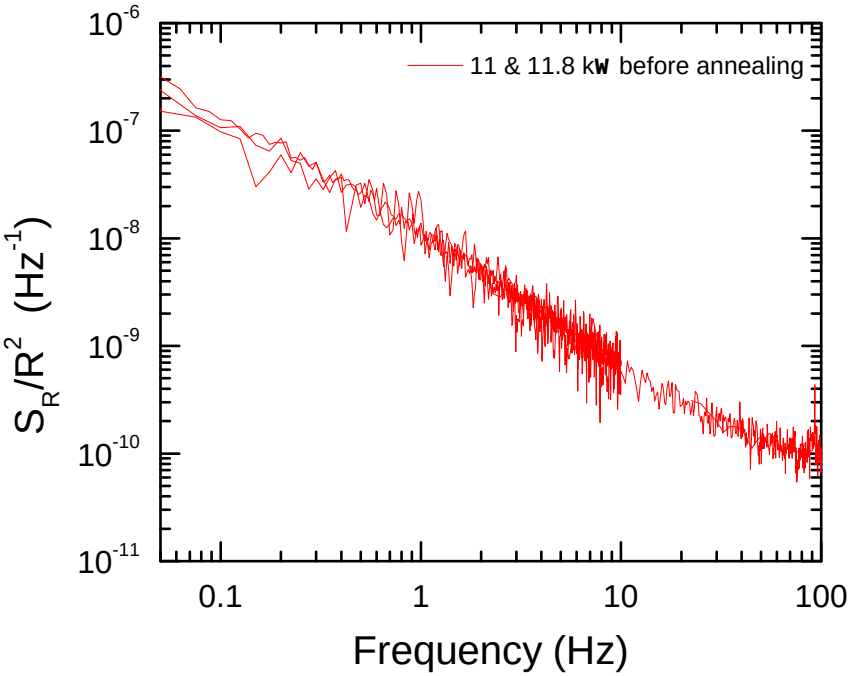

Figure 3.24: Double lock-in cross-correlation measured noise spectrum of tunnel junctions. Samples were fabricated in UHV on SiO-chip and annealing was done at 400°C.

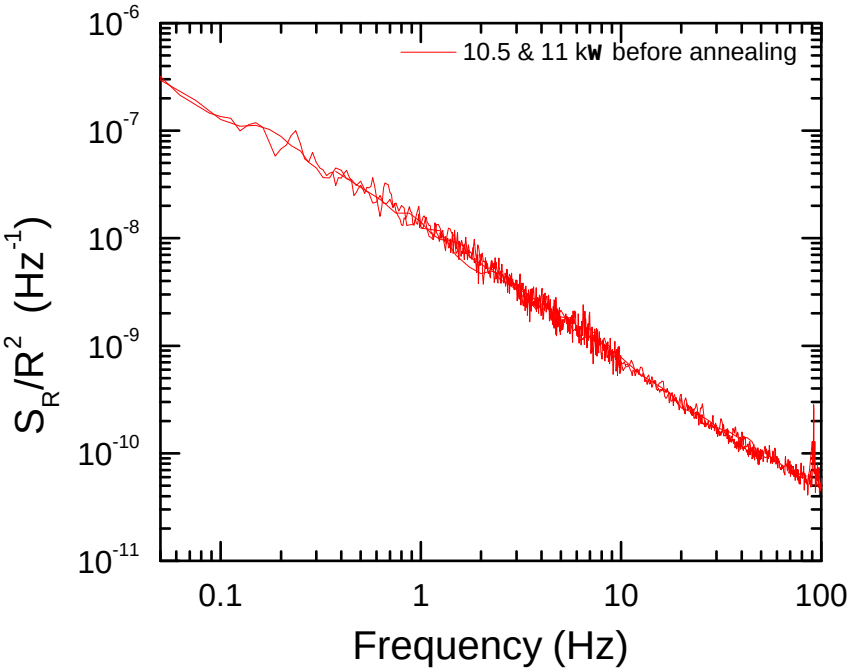

Figure 3.25: Double lock-in cross-correlation measured noise spectrum of tunnel junctions. Samples were fabricated in UHV on SiN-chip and annealing was done at 400°C.

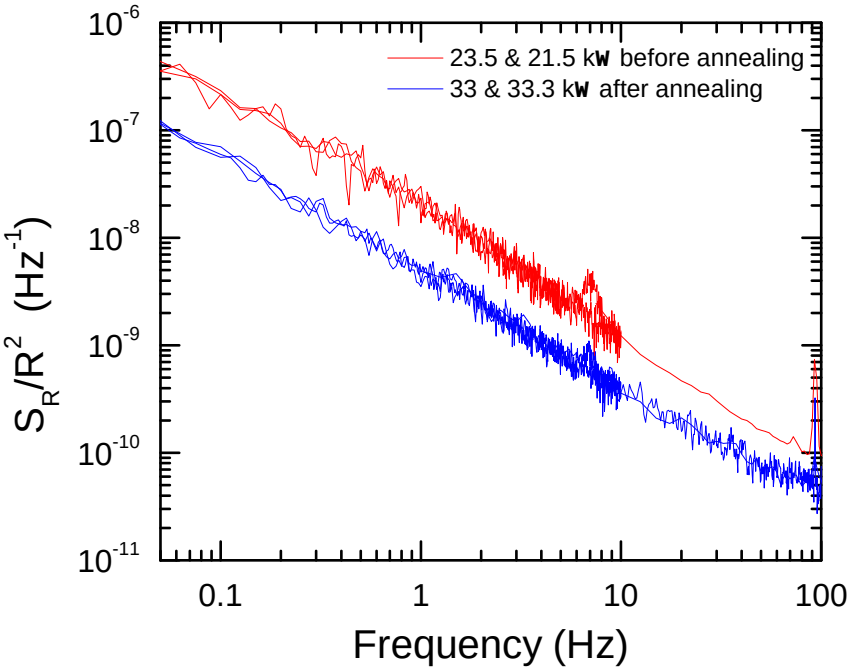

Figure 3.26: Double lock-in cross-correlation measured noise spectrum of tunnel junctions. Samples were fabricated in UHV on SiN-chip and annealing was done at 400°C.

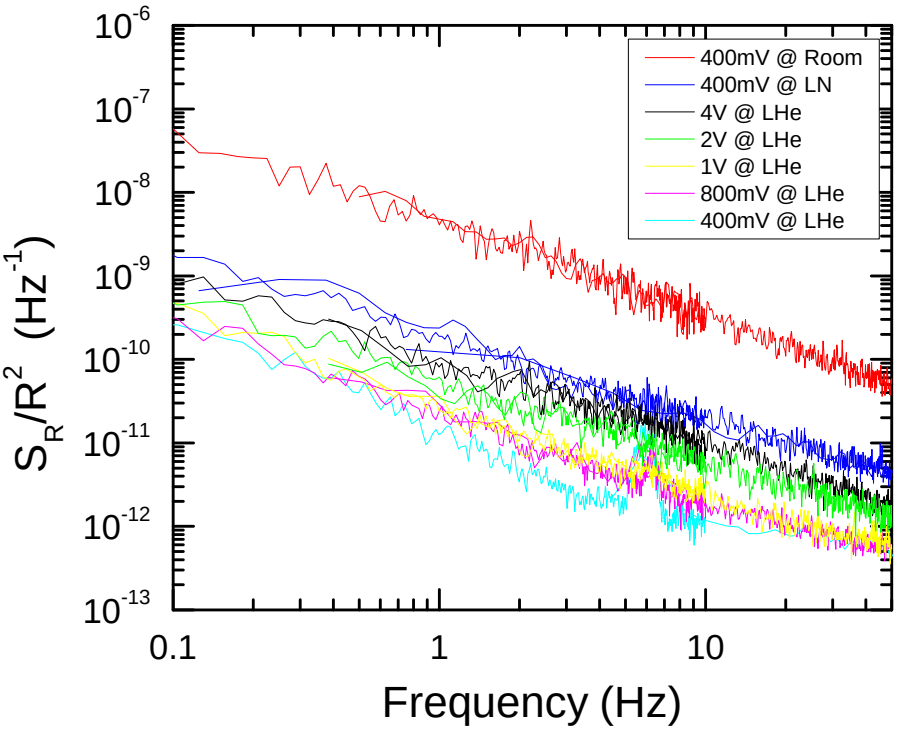

Figure 3.27: Temperature dependence of annealed tunnel junction (the same as in Fig. 3.26) using different cryogenic baths and excitations voltages that might heat up the junction.

compare e.g. Figs. 3.24, 3.25.

The temperature dependence of one annealed sample was measured at a room temperature, in liquid nitrogen (77 K) and in liquid helium (4.2 K). At low temperatures, the 1/f noise decreases rapidly, and to bring the noise level up, higher excitation voltages were used (see Fig. 3.27). Amplitude change is not affecting at higher temperatures than helium bath where the excitation might locally heat up the junction thus providing unreliable data.

Chapter 4

Conclusion

Thermal annealing was found to effectively stabilize all used tunnel junctions. It ceased aging, increased the quality of conductance by reducing resonance peaks and reduced the 1/f noise levels. Percentage drop was 80% in UHV samples and even 90% in HV samples. For further measurements, if more sensitivity is required, the sample impedance should be designed to match with the amplifier specific noise figure i.e. using four PerkinElmer or Ithaco preamplifiers with appropriate impedance transformers.

Interesting phenomena yet not completely studied are dependencies on temperature or sample barrier size and thickness. Here it was found that the noise level depends on junction area. With smaller junction areas the 1/f noises were higher, after normalized by tunneling resistances. One interesting check might be whether the 1/f noise is altered if the junction is suspended, i.e. if there is no substrate at all.

The noise measurement appears to be a sensitive method to study the quality of a tunneling barrier. Metal deposition in the UHV conditions reduced the noise compared to HV fabrication, however, thermal annealing still reduced the noise. It might also be good to check if the noise levels are changing in time, i.e. might there be any kind of aging still remaining.

Bibliography

[1] J. Gallop and F. Piquemal. *The SQUID Handbook*. Wiley-VCH, Weinheim, 2006.

[2] B. Ruggiero, P. Delsing, C. Granata, P. Silvestrini, and Y. Pashkin. *Quantum computing in solid state systems*. Springer, 2005.

[3] J. Bergli, Y. M. Galperin, and B. L. Altshuler. Decoherence in qubits due to low-frequency noise. *New Journal of Physics*, **11**:025002, 2009.

[4] P. J. Koppinen, L. M. Väisto, and I. J. Maasilta. Complete stabilization and improvement of the characteristics of tunnel junctions by thermal annealing. *Applied Physics Letters*, **90**:053503, 2007.

[5] Sh. M. Kogan. *Electronic noise and fluctuations in solids*. Cambridge University Press, Cambridge, 1996.

[6] Paul Horowitz and Winfield Hill. *The art of electronics*. Cambridge University Press, 1989.

[7] J. B. Johnson. Thermal agitation of electricity in conductors. *Phys. Rev.*, **32**:97, 1928.

[8] C. W. J. Beenakker and M. Büttiker. Suppression of shot noise in metallic diffusive conductors. *Phys. Rev. B*, **46**:1889, 1992.

[9] P. Dutta and P. M. Horn. Low-frequency fluctuations in solids: $1f$ noise. *Rev. Mod. Phys.*, **53**:497, 1981.

[10] M. A. Caloyannides. Microcycle spectral estimates of 1/f noise in semiconductors. *J. Appl. Phys.*, **45**:307, 1974.

[11] M. B. Weissman. $1/f$ noise and other slow, nonexponential kinetics in condensed matter. *Rev. Mod. Phys.*, **60**:537, 1988.

[12] F. N. Hooge. 1/f noise is no surface effect. *Physics Letters A*, April 1969.

[13] Michael Tinkham. *Introduction to Superconductivity, 2nd ed.* McGraw-Hill Inc., 1996.

[14] Anssi Lindell. *Nanofabrication by Atomic Force Microscopy, Electron Beam Lithography And Reactive Ion Etching*. PhD thesis, Department of Physics, University of Jyväskylä, 2000.

[15] John G. Simmons. Generalized formula for the electric tunnel effect between similar electrodes separated by a thin insulating film. *J. Appl. Phys.*, **34**:1793, 1963.

[16] R. S. Poikolainen, K. Gloos, and J. P. Pekola. Wide-range thermometer based on thetemperature-dependent conductance. *Appl. Phys. Lett.*, **77**:2915, 2000.

[17] T. A. Fulton and G. J. Dolan. Observation of single-electron charging effects in small tunnel junctions. *Phys. Rev. Lett.*, **59**:109, 1987.

[18] Hermann Grabert and Michel H. Devoret. *Single Charge Tunneling, Coulomb Blockade Phenomena In Nanostructures*. Plenum Press, New York, 1992.

[19] K. T. Loberg, A. J. Manninen, J. P. Kauppinen, and J. P. Pekola. Coulomb blockade thermometer: Tests and instrumentation. *Rev. Sci. Instrum.*, **69**:4166, 1998.

[20] K.P. Hirvi, J.P. Kauppinen, J.P. Pekola, and M.A. Paalanen. Thermometry by arrays of tunnel junctions. *Phys. Rev. Lett.*, **73**:2903, 1994.

[21] V Bouchiat, D Vion, P Joyez, D Esteve, and M H Devoret. Quantum coherence with a single cooper pair. *Physica Scripta*, **T76**:165, 1998.

[22] Mikio Nakahara and Tetsuo Ohmi. *QUANTUM COMPUTING: From Linear Algebra to Physical Realizations*. CRC Press, 2008.

[23] Yuriy Makhlin, Gerd Schön, and Alexander Shnirman. Quantum-state engineering with josephson-junction devices. *Rev. Mod. Phys.*, **73**:357, 2001.

[24] M. Nahum and John M. Martinis. Ultrasensitive-hot-electron microbolometer. *Appl. Phys. Lett.*, page 3075.

[25] *PerkinElmer Model 5184 Preamplifier data sheet.* . http://www.signalrecovery.com/5184page.htm.

[26] *Ithaco Model 1201 Preamplifier data sheet.* . http://www.dlinstruments.com/products/pdf/1201.pdf.

[27] M. Sampietro, L. Fasoli, and G. Ferrari. Spectrum analyzer with noise reduction by cross-correlation technique on two channels. *Rev. Sci. Instrum.*, **70**:2520, 1999.

[28] John H. Scofield. ac method for measuring low-frequency resistance fluctuation spectra. *Rev. Sci. Instrum.*, **58**:985, 1987.